A Bayesian Filtering Approach for Tracking Arousal From Binary and Continuous Skin Conductance Features

Dilranjan S. Wickramasuriya, *Student Member, IEEE*, and Rose T. Faghih, *Member, IEEE*

Abstract*—*Objective: **Neuroanatomical structures within the cortical and sub-cortical brain regions process emotion and cause subsequent variations in signals such as skin conductance and electrocardiography. The signals often encode information in their continuous-valued amplitudes or waves as well as in their underlying impulsive events. We propose to track psychological arousal from this hybrid source of skin conductance information.** ***Methods:*** **We present a point process state-space method in tandem with Bayesian filtering for determining a continuous-valued arousal state from skin conductance measurements. To perform state estimation, we relate arousal to binary- and continuous-valued observations derived from the phasic and tonic parts of a skin conductance signal, and recover model parameters using expectation-maximization. We evaluate our model on both synthetic and two different experimental data sets. Stress was artificially induced in the first experimental data set and the second comprised of a fear conditioning experiment.** ***Results:*** **Results on the first data set indicate high levels of arousal during exposure to cognitive stress and low arousal during relaxation. Plausible results are also obtained in the fear conditioning data set consistent with previous skin conductance studies in similar experimental contexts.** ***Conclusion:*** **The state-space approach—which does not rely on external classification labels—is able to continuously track an arousal level from skin conductance features.** ***Significance:*** **The method is a promising arousal estimation scheme utilizing only skin conductance. The approach could find applications in wearable monitoring and the study of neuropsychiatric conditions such as post-traumatic stress disorder.**

***Index Terms*—State-space methods, Kalman filters, biomedical signal processing, emotion recognition, affective computing.**

I. Introduction

HUMAN emotions are complex and varied. Structures within the brain's limbic system primarily govern emotion [1]. Emotions processed within the central nervous system manifest themselves through several means—most notably through changes in physiological signals, hormone secretions and immune responses [2]. Much attention has been devoted in the literature to examining the relationships between psychological processes and accompanying physiological signal variation patterns. Despite the effort however, significant challenges still remain—especially in the field of automated emotion recognition for wearable monitoring. Wearable emotion monitoring would find applications in stress tracking and the management of emotion-related neuropsychiatric disorders.

Recent efforts in continuous-valued emotion recognition using physiological signals have largely relied on supervised learning techniques based on the Remote Collaborative and Affective Interactions (RECOLA) database [3]. The database contains electrocardiography (EKG) and skin conductance signals acquired from subjects while they engaged in collaborative online tasks. Six annotators subsequently viewed the first 5 min of each of the subjects' video and audio recordings, and manually provided moment-by-moment valence and arousal ratings on a continuous scale between $+1$ and -1. Valence refers to the pleasure-displeasure or positive-negative aspect of an emotion while arousal denotes its corresponding activation [4]. Regression methods for predicting arousal based on the RECOLA database using skin conductance features alone include recurrent neural networks [5], regression trees [6], support vector regression [7], [8] and linear models [9]. Features examined have included basic skin conductance statistics, derivatives, band powers, entropy measures etc. and prediction accuracy is generally reported in terms of a correlation with the ground truth provided by the annotators.

Other affect recognition databases containing physiological signal data have relied on subject scores or population ratings for labels, and do not provide moment-by-moment annotations. The Database for Emotion Analysis using Physiological Signals (DEAP) for instance, provides both self-reported and population arousal and valence scores for each of the minute-long music videos that subjects had to view [10]. Likewise, the Multi-Modal Database for Affect Recognition and Implicit Tagging (MAHNOB-HCI) provides a single arousal and valence score for each movie clip viewed [11]. Such scores have often been separated into the high and low valence and arousal categories (i.e., discrete) for classifying physiological features extracted during each music/video clip. Self-reported scores however,

Manuscript received August 8, 2019; revised September 30, 2019; accepted September 30, 2019. Date of publication October 4, 2019; date of current version May 20, 2020. This work was supported in part by the National Science Foundation under "CRII: CPS: Wearable-Machine Interface Architectures" project under Grant 1755780. R. T. Faghih served as senior author. *(Corresponding author: Rose T. Faghih.)*

D. S. Wickramasuriya is with the Department of Electrical and Computer Engineering, University of Houston.

R. T. Faghih is with the Department of Electrical and Computer Engineering, University of Houston, Houston, TX 77004 USA (e-mail: rtfaghih@uh.edu).

This article has supplementary downloadable material available at http://ieeexplore.ieee.org, provided by the authors.

Digital Object Identifier 10.1109/TBME.2019.2945579

can have significant inter-subject variability [10]. Moreover, experiments such as one whose data is analyzed here—the study of human fear learning through Pavlovian conditioning—do not necessarily conform to the traditional supervised learning paradigm. In this type of experiment, an animal or person gradually learns to associate a neutral stimulus with a more significant one through repeated exposure [12]. Eventually, the neutral stimulus alone begins to elicit a biological response similar to that expected from the non-neutral one. We therefore use a state-space approach that does not rely on external labels. Here, skin conductance features form the observations corresponding to an unobserved emotional state.

Sweat chiefly serves to regulate the body's internal temperature. Despite this primary role played in homeostasis, tiny variations in sweat secretions, and consequently the skin's conductivity, occur in response to arousing stimuli. A skin conductance signal comprises of a slow-varying tonic component and a much faster phasic component [13]. The phasic component consists of multiple skin conductance responses (SCRs) resulting from bursts of underlying sudomotor nerve activity [14]. Each of the SCRs can be modeled as the convolution between an impulse of a certain magnitude and a bi-exponential impulse response function [15]. Multiple studies have attested to the relationship between skin conductance and arousal [16]. The tonic part, also known as the skin conductance level, is thought to capture general autonomic arousal [17], while the SCRs making up the phasic component usually result from sweat expulsions occurring in response to more specific excitement- or arousal-triggered stimuli [14]. Additionally, the tonic and phasic components represent different brain region activity and underlying neural substrates [18]. The tonic level, the SCR peak amplitudes and the rate of the SCRs (caused by bursts of neural firing) are among the features that encode emotion information from the central nervous system. Recovering the neural stimuli causing skin conductance variations thus provides a window into the brain's emotional processes.

Point process state-space (PPSS) methods have been extensively applied to the study of neural spike trains. Application scenarios have included neuroprosthesis [19], [20], movement tracking [21], [22], behavioral learning [23], [24] and the control of medically-induced coma [25]. The depolarization of cells in the heart's sino-atrial node is also similar to the axon potential mechanism in a neuron [26]. Consequently, point process methods have also been applied to the analysis of electrocardiography (EKG) signals (e.g. [27], [28]). PPSS methods have not been solely restricted to the analysis of binary data, but have also been extended to incorporate continuous-valued observations as well. These augmented models incorporate continuous-valued observations such as reaction times and have been again applied to behavioral learning [29]–[31], sleep studies [32], [33] and anesthetic-induced unconsciousness [34], [35].

Neural spike trains underlie the generation of skin conductance signals. Therefore, the point process approach naturally lends itself as tool for skin conductance analysis. However, PPSS methods have only scarcely been applied to the analysis of skin conductance data. In a skin conductance signal, information is not only contained in the SCR occurrences themselves, but rather in the tonic and phasic component amplitudes as well. We therefore propose the use of an extended PPSS model to the study of psychological arousal using skin conductance measurements. We relate three features taken from skin conductance—the binary occurrence or non-occurrence of SCR peaks, the tonic part and a signal derived from the phasic part—to the brain's unobserved arousal state and use Bayesian filtering for estimation. We derive an expectation-maximization (EM) approach to estimate model parameters. The present work is an extension of [36] which only considered the appearance of neural spikes (binary) related to a skin conductance signal. The recent work in [36] is one of the early works for tracking emotion by explicitly making use of the point process methodology.

Section II describes our model formulation and the results are presented thereafter. We next provide a discussion of our results and finally conclude with Section V noting possible future directions.

II. Methods

A. Data

1) Data Set 1 - Neurological Status Assessment: We first used the Non-EEG Data Set for Assessment of Neurological Status [37]. This data set is publicly available through PhysioNet [38], and contains skin conductance, heart rate, body temperature, movement (accelerometer data) and blood oxygenation signals from 20 subjects who were exposed to physical, cognitive and emotional stress. The purpose of the experiment was to probe a subject's neurological stress state using peripheral signals (psychological stress is a function of arousal [39]). The skin conductance, body temperature and accelerometer signals were collected using the Affective Q Curve wearable biosensor. Skin conductance reflects changes in sweat secretions occurring due to sympathetic nervous system arousal [40]. Heart rate and blood oxygenation were acquired using the Nonin Wireless WristOx2 oximeter. Blood oxygen is measured by the saturation percentage of oxygen in hemoglobin (SpO2) and is an indication of how much oxygen is present in the blood. Signals such as skin conductance, heart rate, SpO2 and body temperature show subtle variations during different emotions [41] and have thus frequently been used in the field of affective computing for automated emotion recognition (e.g. [3], [10], [11], [42]). We discarded the physical stress component at the start of the experiment consisting of standing, walking and jogging, and instead focus solely on the psychological and cognitive aspects. The cognitive stress component, which came second, consisted of two tasks—counting backwards in 7's beginning at 2485 and the Stroop test. In a typical Stroop test, subjects are presented with a word on a computer screen denoting a color; the color in which the word is written however, does not necessarily correspond to its semantic meaning. A buzzer notified subjects of mistakes they made while counting or performing the Stroop test. Thirdly and finally, a horror movie clip was used to induce emotional stress. Both the cognitive and emotional stress periods lasted for about 5 min each and were interspersed by 5 min periods of relaxation. Birjandtalab *et al.* [37] noted that the subjects even began showing signs of stress during the 40 s

prior to the cognitive tasks while they were just being given the instructions, and hence chose to include this period among the stressors as well.

2) Data Set 2 - Fear Conditioning: Secondly, we used the PsPM-HRA1: Skin Conductance Responses in Fear Conditioning with Visual CS and Electrical US Data Set [43] containing recordings from 20 subjects who participated in a Pavlovian fear conditioning task. The data set is described in more detail in [44], [45]. A fear conditioning paradigm consists of two types of conditioned stimuli (CS+ and CS−), only one of which (CS+) is followed by an unpleasant unconditioned stimuli (US), such as a shock. The other conditioned stimuli (CS−) is never accompanied by the US. Fear conditioning experiments based on skin conductance acquisition have frequently been used in the study of neuropsychiatric diseases such as post-traumatic stress disorder (PTSD) [46] and panic attacks [47]. In the data set used here, the conditioned stimuli CS+ and CS− were orange and blue circles on a screen. The CS+ stimuli were accompanied by a 0.5 s duration electric shock 50% of the time after a time delay of 3.5 s. The 500 Hz electric shock was delivered to a subject's forearm via a pin-cathode/ring-anode setup. The electric current amplitudes were varied based on individual pain assessment prior to the experiment. There were a total of 180 trials—90 for each CS type. In a typical fear conditioning experiment such as this, the CS+ stimuli alone eventually begin to generate stress responses while the subjects gradually become indifferent to the CS− cues. For each subject, skin conductance was measured using Ag/AgCl cup electrodes placed on the thenar/hypothenar of the subject's non-dominant hand with a constant voltage of 2.5 V applied.

Skin conductance has been extensively examined in classical Pavlovian fear conditioning tasks owing to its sensitivity to sympathetic arousal [16], [48]. Here, a neutral stimulus such as a tone or visual marker is paired with a biological stimulus meant to elicit a response. Through repeated exposure, a subject learns an association between the two types stimuli and eventually begins to respond to the neutral stimulus in a manner similar to that induced by the other. In fear conditioning, the biological stimulus is aversive (e.g. an electric shock). Multiple studies have sought to discover the neural circuitry in the brain underlying fear learning. Although the precise pathways are not fully known, the amygdala and the hippocampus are thought to play a prominent role in processing external sensory inputs and mediating the autonomic and behavioral response to fear [49]. Outputs from these brain regions travel down the spinal cord to the cholinergic sympathetic nerve fibers innervating the sweat glands [50]. Consequently, changes in skin conductance (arising due to sweat secretions) provide an indication of autonomic sympathetic arousal [40]; skin conductance is thus the most widely used measure of autonomic activity in fear conditioning experiments [51].

B. Preprocessing

We downsampled the skin conductance signals from both data sets to 4 Hz similar to [15]. Motion artifacts, powerline noise and amplification factor changes can significantly distort experimental skin conductance measurements [16]. We discarded data from 9 subjects in the neurological status assessment data set containing large discontinuities between consecutive experimental phases and more severe noise contamination. Next, we manually identified sharp drops in the signals (likely caused by electrode movement) and interpolated over them using the preceding and subsequent 1 s of data. Finally, the data was FIR lowpass filtered at 0.5 Hz for smoothing and noise reduction similar to [52]. Skin conductance signals in the fear conditioning data set were similarly filtered although motion artifact correction did not have to be applied. Subject information for both data sets is provided in the supplementary information section. We finally decomposed the skin conductance signals into their constituent tonic and phasic parts using cvxEDA [53].

C. State-Space Model

Random walk models and first order autoregressive processes have been frequently used in the estimation of unobserved dynamic neural states from point process data [23], [31], [32], [54]. Similar to [54] we assume the brain's arousal state x_k follows a first-order autoregressive model

$$x_k = \rho x_{k-1} + \alpha i_k + \varepsilon_k, \tag{1}$$

where $\varepsilon_k \sim \mathcal{N}(0, \sigma_\varepsilon^2)$ is noise and i_k is an indicator function representing external stimuli. Individual SCRs can be isolated by detecting peaks in the phasic part of a skin conductance signal that are above a 0.01–0.05 μS threshold [13]. We detect these SCR peaks based on a minimum peak threshold of 0.015 μS. We next prepare a binary signal $m_k = \{0, 1\}$ based on the non-occurrence or occurrence of an SCR peak at each time index k. The occurrence of such an SCR peak follows a Bernoulli distribution with probability p_k. We therefore apply the theory of generalized linear models to relate it to the arousal state x_k. McCullagh and Nelder [55] suggest the use of the logit, inverse normal or complementary log-log transformation when fitting such a model. Such logarithmic transforms are common in the case where response variables are count or frequency type data. Similar to [23] we use the logit transform.

$$\log\left(\frac{p_k}{1-p_k}\right) = \beta + x_k \Longrightarrow p_k = \frac{1}{1+e^{-(\beta+x_k)}} \tag{2}$$

As in [23], we assume a zero starting state at the very beginning and calculate $\beta = \log[p_0(1-p_0)^{-1}]$ taking p_0 as the average probability that $m_k = 1$ [36]. According to (2), the higher the arousal x_k, the higher will be the probability of SCR occurrence. The increased rate of SCR occurrence as an index of higher autonomic arousal has been attested to in studies involving thought suppression [56], task complexity [57], alcohol consumption [58] and speech processing [59].

We next consider the tonic (s_k) and phasic ($\tilde{r}_k$) components of the skin conductance signal z_k. As mentioned earlier, changes in the tonic component are thought to "reflect general changes in autonomic arousal" [17]. The tonic level has also been taken as a measure of arousal in studies involving anti-social behavior [60], thought suppression [61], alcohol consumption [58] and personality types [62]. Higher tonic levels indicate higher

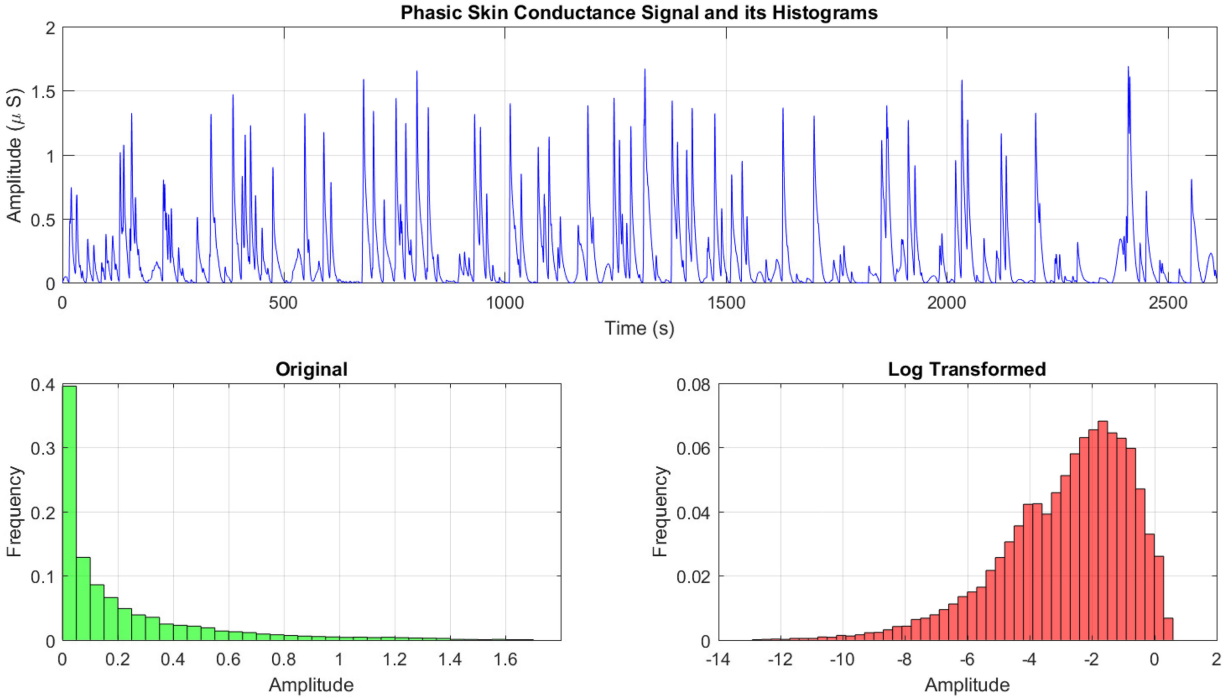

Fig. 1. A phasic skin conductance signal and its histograms. The upper sub-panel depicts the phasic component of the skin conductance signal from subject 1 in the fear conditioning data set. The lower left sub-panel shows its histogram and the right sub-panel the same after a log transformation has been applied. The transformation significantly improves skewness of the phasic component.

arousal. Continuous observations are frequently modeled as being linearly related to unobserved states in augmented PPSS methods [30], [31]. We too take s_k to be related to x_k as follows:

$$s_k = \delta_0 + \delta_1 x_k + w_k, \tag{3}$$

where δ_0, δ_1 are regression coefficients to be determined, and $w_k \sim \mathcal{N}(0, \sigma_w^2)$ represents sensor noise and modelling error.

The phasic component $\tilde{r}_k$, which consists of the entire sequence of SCRs, unlike its tonic counterpart, is significantly skewed. A log transformation [16] helps correct this skew (Fig. 1). Moreover, arousal is related to the SCR peak amplitudes [63] rather than to $\tilde{r}_k$ as a whole. SCR amplitudes have been used as indicators of psychological arousal in studies involving emotional sounds [64] and pictures [65]. Again, higher SCR amplitudes reflect higher arousal. In order to both improve skewness and capture arousal information from the peak amplitudes, we derive an artificial signal r_k in two steps. We first select only the subset of SCR peak amplitudes along with the first ($\tilde{r}_1$) and last ($\tilde{r}_K$) values

$$r^* = \{\tilde{r}_k | m_k = 1\} \cup \{\tilde{r}_1, \tilde{r}_K\}. \tag{4}$$

Then we apply a cubic interpolation over $\log r^*$ to make up r_k. Fig. 2 depicts the derivation of r_k from $\tilde{r}_k$ on some sample data. Similar to (3) we finally model,

$$r_k = \gamma_0 + \gamma_1 x_k + v_k, \tag{5}$$

where γ_0, γ_1 are to be determined and $v_k \sim \mathcal{N}(0, \sigma_v^2)$ represents an error term similar to w_k. The three observations m_k, r_k and s_k that are finally extracted from a skin conductance signal are illustrated in Fig. 3. Note that the tonic level, the SCR rate and the

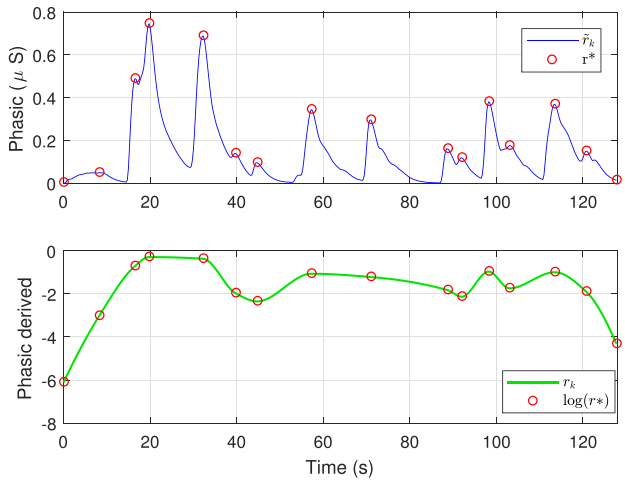

Fig. 2. Deriving r_k from $\tilde{r}_k$. The upper sub-panel depicts the phasic component $\tilde{r}_k$ along with the points r^* consisting of the values at either end and the peaks. The lower sub-panel depicts the cubic interpolated line joining $\log r^*$ which makes up r_k.

SCR amplitude are among the most reported skin conductance-related measures of arousal [41].

Given the observations $\mathcal{M}^K = \{m_1, m_2, \ldots, m_K\}$, $\mathcal{R}^K = \{r_1, r_2, \ldots, r_K\}$, $\mathcal{S}^K = \{s_1, s_2, \ldots, s_K\}$, and letting $\mathcal{Y}^K = \{\mathcal{M}^K, \mathcal{R}^K, \mathcal{S}^K\}$, we wish to determine $\mathcal{X}^K = \{x_1, x_2, \ldots, x_K\}$. To do so, we use Bayesian filtering within an EM framework. In the E-step, we first obtain the estimates of $\mathcal{X}^K$ conditioned on $\mathcal{Y}^K$ and the model parameters $\{\alpha, \rho, \gamma_0, \gamma_1, \delta_0, \delta_1, \sigma_v^2, \sigma_w^2, \sigma_\varepsilon^2\}$. In the M-step, we choose the model parameters that maximize the expected value of the

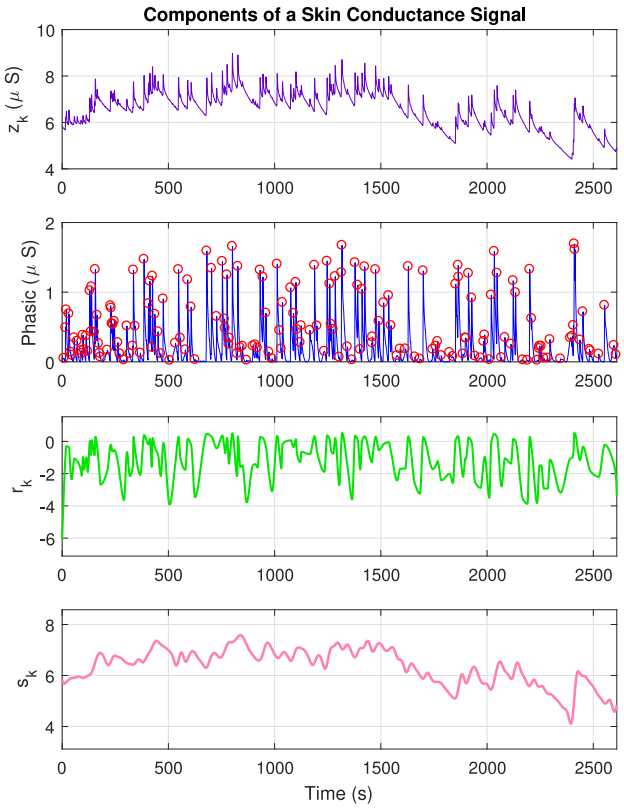

Fig. 3. A skin conductance signal and its constituent components. The sub-panels from top to bottom respectively depict the original skin conductance signal z_k, the phasic part with its SCR peaks (m_k indicates the peak occurrences), the phasic derived component r_k and the tonic part s_k.

complete data log-likelihood. The algorithm alternates between the E-step and the M-step until convergence. The following sub-sections describe the E- and M-steps.

D. Estimation – E-Step

We estimate $\mathcal{X}^K$ in two steps using both a forward filter and a backward smoother. We first make a Gaussian approximation (supplementary information) to the posterior distribution $p(x_k|y^k)$ similar to [29], [31] in order to obtain the following Kalman-like filter equations for $k = 2 : K$.

$$x_{k|k-1} = \rho x_{k-1|k-1} + \alpha i_k \tag{6}$$

$$\sigma^2_{k|k-1} = \rho^2 \sigma^2_{k-1|k-1} + \sigma^2_\varepsilon \tag{7}$$

$$C_k = \frac{\sigma^2_{k|k-1}}{\sigma^2_v \sigma^2_w + \sigma^2_{k|k-1}(\gamma_1^2 \sigma^2_w + \delta_1^2 \sigma^2_v)} \tag{8}$$

$$\begin{aligned} x_{k|k} = x_{k|k-1} + C_k \Big[& \sigma^2_v \sigma^2_w (m_k - p_{k|k}) \\ & + \gamma_1 \sigma^2_w (r_k - \gamma_0 - \gamma_1 x_{k|k-1}) \\ & + \delta_1 \sigma^2_v (s_k - \delta_0 - \delta_1 x_{k|k-1}) \Big] \end{aligned} \tag{9}$$

$$\sigma^2_{k|k} = \left[\frac{1}{\sigma^2_{k|k-1}} + p_{k|k}(1 - p_{k|k}) + \frac{\gamma_1^2}{\sigma^2_v} + \frac{\delta_1^2}{\sigma^2_w} \right]^{-1} \tag{10}$$

Now,

$$p_{k|k} = \frac{1}{1 + e^{-(\beta + x_{k|k})}} \tag{11}$$

causes $x_{k|k}$ to appear on both sides of (9) and has to be solved numerically via the Newton-Raphson method [23]. Similar to a Kalman filter update step, (9) contains innovation terms for the continuous variables r_k and s_k and also a term comparing the binary value m_k to its predicted probability $p_{k|k}$. The smoothed estimates $x_{k|K}$ and $\sigma^2_{k|K}$ conditioned on having observed all the data up to time index K are obtained as [23], [66],

$$a_k \triangleq \rho \frac{\sigma^2_{k|k}}{\sigma^2_{k+1|k}} \tag{12}$$

$$x_{k|K} = x_{k|k} + a_k (x_{k+1|K} - x_{k+1|k}) \tag{13}$$

$$\sigma^2_{k|K} = \sigma^2_{k|k} + a_k^2 (\sigma^2_{k+1|K} - \sigma^2_{k+1|k}). \tag{14}$$

E. Estimation – M-Step

The parameters $\{\alpha, \rho, \gamma_0, \gamma_1, \delta_0, \delta_1, \sigma^2_v, \sigma^2_w, \sigma^2_\varepsilon\}$ are determined in the M-step. These parameters are selected to maximize the expected value of the complete data log-likelihood (we derive the M-step updates in the supplementary information). We make use of the state-space covariance algorithm when deriving our parameter estimates [67]. Defining the following terms,

$$u_k \triangleq x^2_{k|K} + \sigma^2_{k|K} \tag{15}$$

$$u_{k,k+1} \triangleq x_{k|K} x_{k+1|K} + a_k \sigma^2_{k+1|K} \tag{16}$$

we obtain the following parameter estimates for the $(n+1)$th EM iteration.

$$\begin{aligned} \begin{bmatrix} \rho^{(n+1)} \\ \alpha^{(n+1)} \end{bmatrix} = & \begin{bmatrix} \sum_{k=1}^{K-1} u_k & \sum_{k=2}^{K} i_k x_{k-1|K} \\ \sum_{k=2}^{K} i_k x_{k-1|K} & \sum_{k=1}^{K} i_k^2 \end{bmatrix}^{-1} \\ & \times \begin{bmatrix} \sum_{k=1}^{K-1} u_{k,k+1} \\ \sum_{k=2}^{K} i_k x_{k|K} \end{bmatrix} \end{aligned} \tag{17}$$

$$\begin{aligned} \begin{bmatrix} \gamma_0^{(n+1)} \\ \gamma_1^{(n+1)} \end{bmatrix} = & \begin{bmatrix} K & \sum_{k=1}^{K} x_{k|K} \\ \sum_{k=1}^{K} x_{k|K} & \sum_{k=1}^{K} u_k \end{bmatrix}^{-1} \\ & \times \begin{bmatrix} \sum_{k=1}^{K} r_k \\ \sum_{k=1}^{K} r_k x_{k|K} \end{bmatrix} \end{aligned} \tag{18}$$

$$\begin{aligned} \sigma_v^{2(n+1)} = \frac{1}{K} \Bigg[& \sum_{k=1}^{K} r_k^2 + K\gamma_0^{2(n+1)} + \gamma_1^{2(n+1)} \sum_{k=1}^{K} u_k \\ & - 2\gamma_0^{(n+1)} \sum_{k=1}^{K} r_k - 2\gamma_1^{(n+1)} \sum_{k=1}^{K} x_{k|K} r_k \\ & + 2\gamma_0^{(n+1)} \gamma_1^{(n+1)} \sum_{k=1}^{K} x_{k|K} \Bigg] \end{aligned} \tag{19}$$

TABLE I
PARAMETER ESTIMATION WITH SIMULATED DATA

Θ	$\hat{\Theta}$ ($\hat{p}_0 < 0.01$)	$\hat{\Theta}$ ($\hat{p}_0 > 0.01$)
$\alpha = 0.04$	0.018	0.021
$\rho = 0.995$	0.994	0.994
$\beta_0 = -4.595$	-4.64	-4.057
$\gamma_0 = 0.35$	0.233	0.608
$\gamma_1 = 0.4$	0.450	0.377
$\delta_0 = -0.7$	-0.758	-0.571
$\delta_1 = 0.2$	0.224	0.187
$\sigma_V^2 = 0.002$	0.0022	0.0016
$\sigma_W^2 = 0.005$	0.0046	0.0050
$\sigma_\varepsilon^2 = 0.03$	0.0219	0.0216

$$\sigma_\varepsilon^{2(n+1)} = \frac{1}{K}\Bigg[\sum_{k=2}^{K} u_k - 2\rho^{(n+1)}\sum_{k=1}^{K-1} u_{k,k+1} + \rho^{2(n+1)}\sum_{k=1}^{K-1} u_k - 2\alpha^{(n+1)}\sum_{k=2}^{K} i_k x_{k|K} + 2\alpha^{(n+1)}\rho^{(n+1)}\sum_{k=2}^{K} i_k x_{k-1|K} + \alpha^{2(n+1)}\sum_{k=1}^{K} i_k^2\Bigg] \tag{20}$$

The M-step updates for $\delta_0^{(n+1)}$ and $\delta_1^{(n+1)}$ can be obtained by replacing r_k with s_k in (18). Likewise, $\sigma_w^{2(n+1)}$ can be obtained similar to (19).

III. RESULTS

A. Simulated Data

We first generated some synthetic data for an arousal state process x_k to check the convergence of our EM approach using the parameters $\Theta = \{\alpha, \rho, \beta, \gamma_0, \gamma_1, \delta_0, \delta_1, \sigma_v^2, \sigma_w^2, \sigma_\varepsilon^2\} = \{0.04, 0.995, -4.595, 0.35, 0.4, -0.7, 0.2, 0.002, 0.005, 0.03\}$. These values were chosen based on prior experience with experimental data. We arbitrarily set $i_k = 1$ at 25 time instances and 0 elsewhere. The EM stopping criteria is similar to [23], [30] and we consider the parameters to have converged once their absolute mean deviation in consecutive iterations does not exceed 10^{-8}.

Recall that we calculate $\beta = \log[p_0(1-p_0)^{-1}]$ using an approximation for p_0 as the average probability that $m_k = 1$ [36]. We call this approximate probability $\hat{p}_0$. The value chosen for β in the synthetic data corresponds to $p_0 = 0.01$, i.e., $\beta = \log[0.01(1-0.01)^{-1}]$. We generated two synthetic data sets for which the approximation $\hat{p}_0$ was lower than, and then higher than 0.01. The recovered model parameters $\hat{\Theta}$ are shown in Table I. The state estimates and fits to the observed data are shown in Fig. 4 and in the supplementary information. While our proposed scheme can recover model parameters and estimate x_k reasonably well, the less-than-true approximation ($\hat{p}_0 < 0.01$) causes the state x_k to be overestimated by an almost constant amount (Fig. 4) and the higher-than-true approximation ($\hat{p}_0 > 0.01$) causes x_k to be slightly underestimated (supplementary information). A note on how the effect of this can be mitigated on experimental data is made in the subsequent discussion section.

B. Experimental Skin Conductance Data

When using the proposed model on experimental skin conductance data, the EM algorithm can converge to parameters where the shape of x_k fits almost perfectly to either r_k or s_k. It is likely that there are two locally optimal points in the model parameter space at these locations. However, we would like the arousal state to fit to *both* the tonic and phasic-derived components capturing the neural dynamics underlying each of them. Recall that both the phasic and tonic parts represent different neural activity from different parts of the brain [18], and we would like to capture arousal information from both regions. Additionally, the tonic component captures general arousal while the phasic captures arousal related to specific stimuli. With the near-perfect shape alignment of x_k only to one of them, either σ_v^2 or σ_w^2 is driven very low at the expense of the other. Therefore, we divide r_k and s_k by their respective standard deviations and allow the parameters related just to them, i.e. $\{\gamma_0, \gamma_1, \delta_0, \delta_1, \sigma_v^2, \sigma_w^2\}$, to update at a given M-step iteration only if the absolute difference between $\sigma_v^{2(n+1)}$ and $\sigma_w^{2(n+1)}$ is less than 0.1. This heuristic constraint helped prevent x_k from overfitting only to one of them.

1) Data Set 1 - Neurological Status Assessment: Since the precise timings of the stimuli (i.e., Stroop test word appearances and buzzer sounds) are not provided in the neurological status assessment data set, we drop the αi_k term from (1). The state estimates and fits to the binary- and continuous-valued observations for a representative subject are shown in Fig. 5. Due to space limitations, the results for the remaining subjects are provided in the supplementary information. The shaded background colors in turn correspond to relaxation, the cognitive stress period (instructions, counting backwards and the Stroop test), relaxation, the emotional stress period (horror movie) and relaxation. We have also chosen to show the fits for e^{r_k} rather than to the artificial r_k in the figures as it is the exponential term that is actually closer to the physiological phasic component.

x_k lies in the interval $(-\infty, \infty)$. We therefore adapt the certainty level measurement in [23], [30] and define a new quantity which we call the Above-Moderate Arousal Index (AMAI) as an additional metric that may be more useful to a wearable device user. We define AMAI as the probability that x_k exceeds a subject-specific threshold using $x_k \sim \mathcal{N}(x_{k|K}, \sigma_{k|K}^2)$ at each time point.

$$\text{AMAI} = P(x_k > x_{th}), \tag{21}$$

where x_{th} is a fixed subject-specific threshold. AMAI can, for instance, provide a score related to how aroused a person is above their median baseline. The greater a person's arousal, the more the probability distribution of x_k shifts to the right giving a high AMAI value. We selected this threshold x_{th} using a Receiver Operating Characteristic (ROC) curve considering the

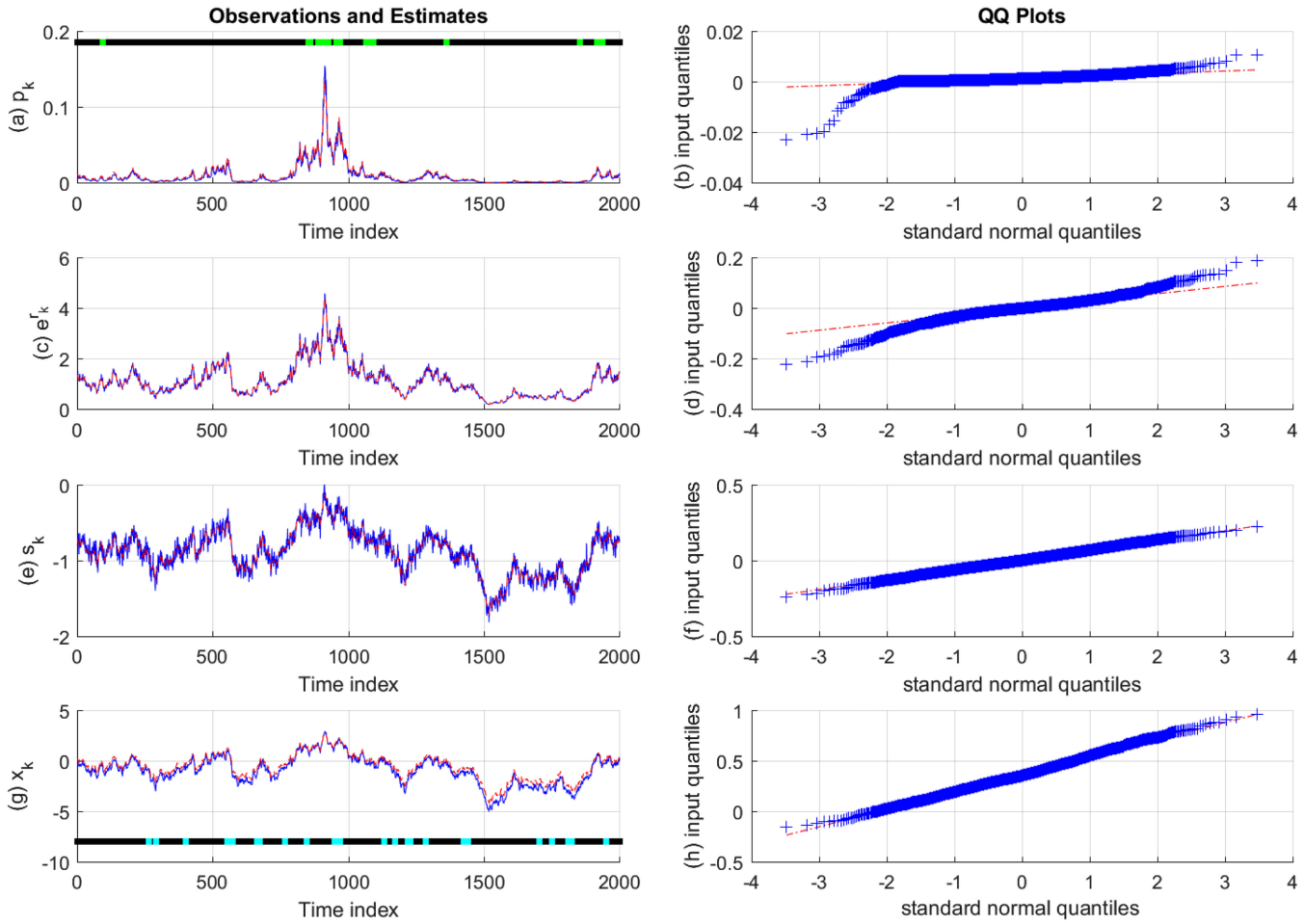

Fig. 4. Arousal state estimation on synthetic data for $\hat{p}_0 < 0.01$. The sub-panels respectively depict, (a) the original Bernoulli trial probabilities p_k (solid blue line), their estimate (red dashed line) and the presence or absence of binary observations (light green and black dots above the curve); (b) the quantile-quantile (QQ) plot for the residual error of p_k; (c) the exponent of the first continuous signal r_k (solid blue line) and its estimate (red dashed line); (d) the QQ plot for the residual error of r_k; (e) the second continuous signal s_k (solid blue line) and its estimate (red dashed line); (f) the QQ plot for the residual error of s_k; (g) the arousal state x_k (solid blue line), its estimate (red dashed line) and the presence or absence of stimuli i_k driving the state (cyan and blacks dots below the curve); (h) the QQ plot for the residual error of x_k.

x_k values during cognitive stress to belong to the positive class and the values during all the relaxation periods to belong to the negative class. The emotional stress period does not appear to have a consistent pattern across all subjects and therefore we discarded it from either class when identifying the threshold. The area under the curve (AUC) for each ROC curve is shown in Table II and the three-level color-coded AMAIs appear in the last of the sub-panels for each participant. The three regions (colors) correspond to AMAI ≤ 0.1 (green), $0.1 <$ AMAI ≤ 0.9 (blue) and $0.9 <$ AMAI (red).

The time period shown here begins a minute before the cognitive stress phase commences. The general trend to be noted for all the subjects is an initial rise in the arousal state x_k to a level at which it remains high during cognitive stress, and thereafter reduces gradually as the experiment progresses. The initial increase is quite rapid for a majority of the subjects but is more gradual for participants 8, 9 and 11. During cognitive stress, arousal remains high and comparatively steady for participants 5 and 10. The others exhibit some variations during this period.

TABLE II
CLASSIFICATION ACCURACY OF NEUROLOGICAL STATUS ASSESSMENT DATA SET

Participant	AUC
1	0.9596
2	0.7917
3	0.7287
4	0.9847
5	0.8935
6	0.9217
7	0.9674
8	0.8020
9	0.9027
10	0.9576
11	0.8257

There is a gradual decline in x_k for everyone after the cognitive stress period is over. There are however, some fluctuations in arousal for participants 3 and 6 during the relaxation period that immediately follows cognitive stress.

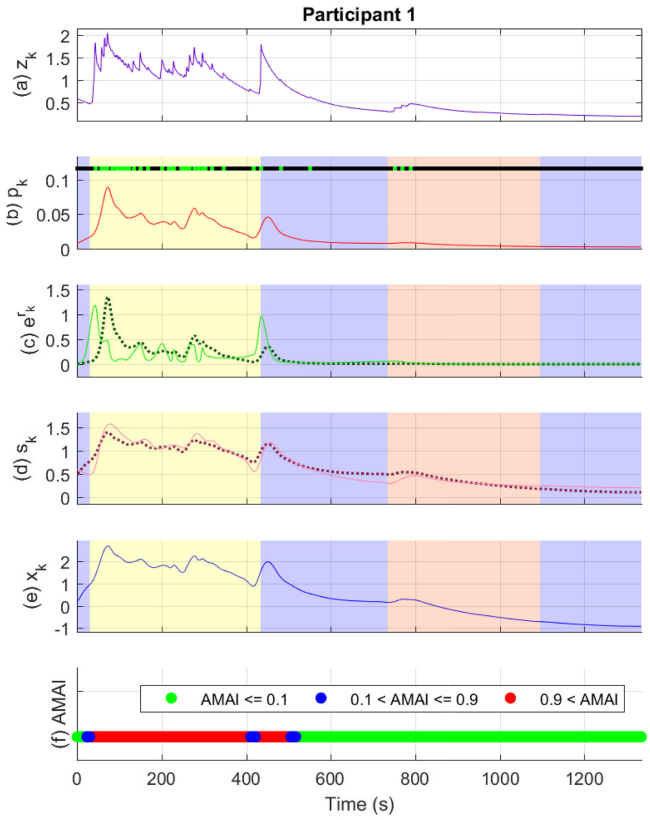

Fig. 5. Arousal state estimation on the neurological status assessment data set. The sub-panels from top to bottom respectively depict, (a) the original skin conductance signal; (b) the smoothed Bernoulli trial probability estimates of p_k (red line) and the presence or absence of SCR peaks (light green and black dots above the curve); (c) the exponent of the phasic derived signal r_k (solid green line) and its estimate (dotted line); (d) the tonic component s_k (solid light mauve line) and its estimate (dotted line); (e) the smoothed arousal state estimates of x_k; (f) the color-coded AMAI values. The shaded backgrounds correspond in turn to relaxation, cognitive stress, relaxation, emotional stress, and relaxation.

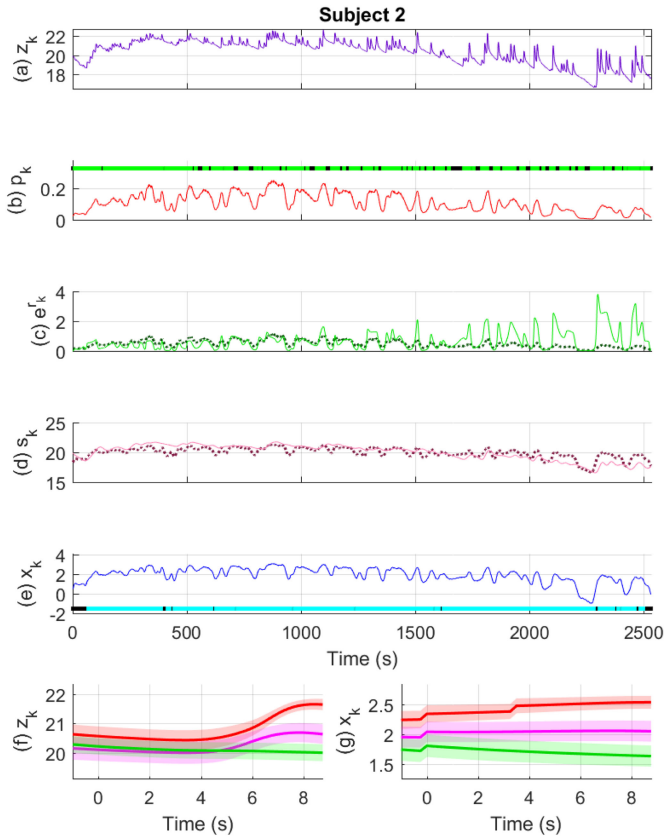

Fig. 6. Arousal state estimation on the fear conditioning data set. The sub-panels from top to bottom respectively depict, (a) the original skin conductance signal; (b) the smoothed Bernoulli trial probability estimates of p_k (red line) and the presence or absence of SCR peaks (light green and black dots above the curve); (c) the exponent of the phasic derived signal r_k (solid green line) and its estimate (dotted line); (d) the tonic component s_k (solid light mauve line) and its estimate (dotted line); (e) the smoothed arousal state estimates of x_k and the presence or absence of visual or electric stimuli (cyan of blacks dots below the curve); (f) a 10 s ERP-like skin conductance plot for the CS− (green), CS+ without a shock (mauve) and CS+ with the shock (red) trials; (g) 10 s ERP-like arousal state plots along with their confidence intervals.

The arousal response is more varied during the emotional stress (horror movie) period. It is to be noted primarily, that with the possible exception of participant 3, arousal during the emotional stress period is lower than it was during cognitive stress. Participants 8, 9, 10, and 11 show almost no fluctuations in arousal during this phase. For participants 1, 2 and 5 there is a slight increase (similar to a bump) around the beginning of emotional stress. For participants 4, 6 and 7 there is more fluctuation during this period. Arousal is seen to decrease thereafter during the final period of relaxation. The color coded AMAIs also tend to follow the general trend of x_k.

2) Data Set 2 - Fear Conditioning: We set $i_k = 1$ at the external CS+, CS− and US stimuli time instances, and $i_k = 0$ elsewhere. An additional constraint was also placed to ensure that α did not become negative in the EM iterations. The result for a representative subject is shown in Fig. 6 and the remaining results are given in the supplementary information.

Since the fear conditioning experiment is in a category similar to the study of event-related potentials (ERPs) using electroencephalography signals, we provide the 10 s ERP-like images averaged across the three different types of trials (CS+ without the shock, CS+ with the shock and CS−). Each epoch begins 1 s prior to the CS+ or CS− visual stimuli and extends to 9 s following it.

Previous fear conditioning studies examining SCR probabilities, SCR amplitudes and skin conductance levels have majorly focused on differences in these observations between the CS+ and CS− trials (e.g. [68], [69]). In the data set used here, the general observation is that both the skin conductance z_k and the estimated state x_k are higher when CS+ is accompanied by the shock. The values are lowest mostly for CS−. This trend is consistent with skin conductance results from previous studies. The averaged differences between the responses are pronounced for subjects 1, 2, 5, 6, 9, 10, 12, 15, 18, 19 and 20. In the case of some of the other subjects however, the difference between the CS- epochs and CS+ without-the-shock epochs are very small. Possible reasons for this are discussed in the following section. It is to be noted however, that when the difference between the averaged skin conductance epochs is small for the three con-

ditions, the difference between the corresponding state epochs also tends to be small.

IV. Discussion

A. Simulated Data

The calculation for β using the approximation for p_0 causes the true state to be over- or underestimated by a certain amount. Now, the estimated arousal state is a real-valued quantity and *relative* increases are of importance in experimental data. Moreover, the AMAI provides a means of calculating a more useful metric based on a person-specific threshold. The effect of the over- or underestimation can be mitigated by the use of such *person-specific* thresholds on wearable devices. A second option would be to obtain the range of variation for a subject's arousal during a calibration or training phase and normalize subsequent values after dividing by this range.

B. Experimental Data

Different people are impacted by identical stressful stimuli differently. In the neurological status assessment data set, a fairly consistent pattern was observed of high arousal during the cognitive stress period and low arousal during relaxation. The horror movie (emotional stress) generated some amount of arousal in the subjects, but was not as pronounced/high as during the cognitive tasks. The backward counting task and Stroop test involved *active* engagement on the part of the subjects requiring them to concentrate and perform calculations. In contrast, the horror movie only involved *passive* engagement with the subjects just having to look at a screen. It is therefore not unexpected that the varying levels of engagement accompanying both types of external stressors elicited different arousal responses. A few participants appeared to show some degree of arousal at the beginning of the movie and others were completely indifferent to it. This may have been due to prior familiarity with the clip being shown. It is also to be noted that some subjects arousal levels rise (and fall) more rapidly than others possibly owing to some of them becoming stressed more easily.

Additionally, although both the counting task and the Stroop test were grouped under the same category called cognitive stress, some subjects show higher levels of arousal during the Stroop test than during the counting task (e.g. participants 8 and 11). This may have been the case for subjects who found arithmetic calculations easier than the color-word visual processing task.

State estimation results from the fear conditioning data set are also as expected. The CS+ stimuli accompanied by the electric shock tend to generate the highest level of arousal. In fear learning experiments, electric shocks that are not unpleasant enough can occasionally cause a subject not to fear the CS+ stimuli. In such cases, a clear separation in z_k and x_k between the three different types of epochs may not necessarily occur as would typically be expected. Bach *et al.* [44] describe how pain and discomfort thresholds were assessed for the subjects in the experiment before finally setting the electric shock intensity just *below* each individual's pain threshold. Pain thresholds can vary from person to person and therefore may be the one of the causes for the variations seen in the z_k and x_k separations.

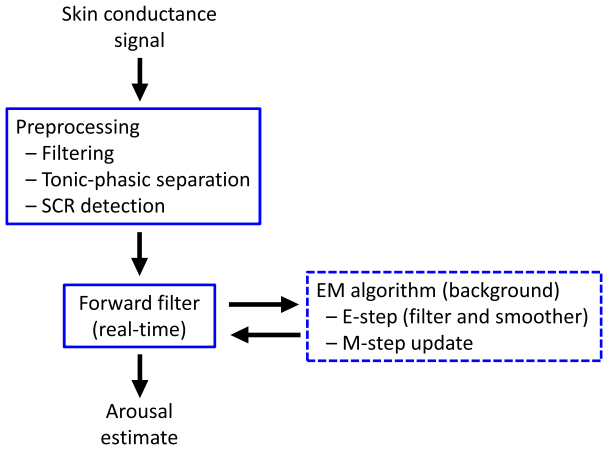

Fig. 7. Flowchart of arousal estimation. The raw skin conductance signal is first filtered and then separated into its constituent tonic and phasic components at the preprocessing stage. SCR peaks are also detected in the phasic component at this stage. The forward filter at the next stage provides the real-time arousal estimate. The full EM algorithm is only executed in the background from time to time to update model parameters.

The CS+, CS− and US stimuli are all different. Therefore, a more comprehensive model for fear conditioning would be

$$x_k = \rho x_{k-1} + \alpha_{CS+} i_k^{CS+} + \alpha_{CS-} i_k^{CS-} + \alpha_{US} i_k^{US} + \varepsilon_k, \tag{22}$$

with *stimulus-specific* α coefficients. Here, we have treated all the stimuli the same with a single α term and $i_k = 1$ at each of the stimuli instances. We leave an extended model with stimulus-specific terms for future work.

We also evaluated the state-space model on the fear conditioning data set without the i_k term. This provided almost identical results to that with the i_k included, except for the jumps seen at the times when stimuli were presented. The inclusion of external input provides additional information to the model. PPSS methods with [54] and without [70] external inputs in the state equation have been successfully applied to the analysis of spiking neural activity. PPSS methods without external inputs have also met with success in estimating behavioral learning [23]; however, the inclusion of external inputs has been suggested as an improvement [24]. The external input affecting psychological arousal x_k is likely quite complex (e.g. stress and excitement may affect arousal in different ways). Here, we have considered one of the simplest cases where we set $i_k = 0$ or $i_k = 1$ based on spontaneous inputs in the fear conditioning data set. Smith *et al.* [54] too modeled the external input as a binary indicator in spike train analysis. Stimulus timings are unavailable in the neurological status assessment data set and we were unable to include the i_k effect.

The EM approach presented here is offline as it requires all the observations $\mathcal{Y}^K = \{\mathcal{M}^K, \mathcal{R}^K, \mathcal{S}^K\}$ upon which to run the E-step and M-step until convergence. Therefore, on a wearable device, we propose to run just the forward filter in the E-step,

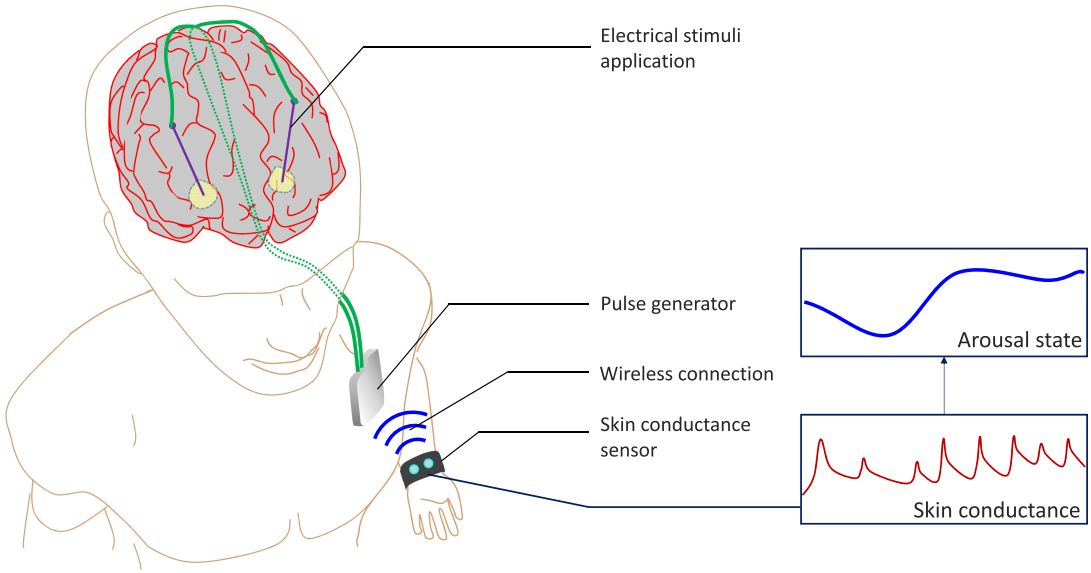

Fig. 8. A closed-loop DBS architecture based on skin conductance feedback. DBS has been investigated as a treatment option for major depression and PTSD. Depression typically involves low levels of arousal [71] while PTSD involves hyperarousal [72]. Skin conductance can be used in the feedback path of a closed-loop DBS system for automatically adjusting electrical stimulation parameters when treating disorders of psychological arousal; figure adapted from [73].

and only execute the full EM procedure in the background from time to time (Fig. 7). A wearable device user would then be able to see his/her arousal estimate $x_{k|k}$ in real-time. Additionally, running EM periodically would allow the model parameters to adapt to different circumstances. Our current implementation on average takes 3.12 s to run on Data Set 1 and 6.5 s on Data Set 2 for a subject (MATLAB R2017a, Intel Xeon processor, 64 GB RAM). Since the time consumption will be much greater on a low-power wearable device, another option would be to stream all the data to the internet and perform all analysis on the cloud to conserve battery power. Cloud data analysis however, is likely to introduce communication latency. The amount of delay that can be tolerated would be application specific. For instance, depression typically involves prolonged periods of low arousal [71] while PTSD involves symptoms of hyperarousal (e.g. angry outbursts) [72]. A longer delay would be tolerable in the case of depression while a much shorter delay would be ideal in the case of a PTSD patient. While further research would be necessary, a latency of less than a minute would be preferable when tracking arousal.

Deep brain stimulation (DBS) has been investigated in a number of neuropsychiatric disorders including major depression and PTSD. Open-loop DBS systems involve the periodic manual adjustment of electrical stimulation parameters based on symptoms. This is inefficient and has led to the gradual development of closed-loop DBS. A method to detect arousal from skin conductance could be used in the feedback path for automatically adjusting electrical stimulation in a closed-loop DBS system for patients diagnosed with PTSD or major depression [73] (Fig. 8).

Recurrent Neural Networks (RNNs) based on Long Short Term Memory (LSTM) units are able to model nonlinear input-output relationships, and capture long-term dependencies in sequential data (e.g. [74]). Our current state-space formulation follows first-order Markovian dynamics and does not have any nonlinear state transitions. This is a simplifying assumption, and we consider a future extension to our work where an RNN is used to learn the relationship $x_k = g(x_{k-1}, i_k) + \varepsilon_k$, where $g(\cdot)$ is an arbitrary function. Evaluating $\bar{Q} = \mathbb{E}_{\mathcal{X}^K|\mathcal{Y}^K,\Phi} \log\left[p(\mathcal{X}^K \cap \mathcal{Y}^K|\Phi)\right]$ is a critical step in the EM algorithm, where Φ represents a set of model parameters (e.g. weights of an RNN or model parameters such as are used in this work). Following [75]–[77], we propose to use a stochastic form of EM where an LSTM-based RNN maximizes $\bar{Q}$ by gradually learning the posterior probability density function $p(\mathcal{X}^K|\mathcal{Y}^K, \Phi)$ through gradient ascent. With this extension, the RNN is able to estimate the unknown states x_k. This allows the interpretability of the state-space method to be fused with the powerful nature of RNNs to capture nonlinear relationships over longer time windows. Future work would involve evaluating and comparing the performance of the state-space method presented here with the RNN-state-space fusion approach.

V. Conclusion

PPSS methods have been extensively applied to neural and EKG data analysis due to the point process nature of the signals. A neural spike train underlies the generation of a skin conductance signal, and therefore PPSS methods lend themselves naturally as convenient tools for their analysis. Here we presented a model for tracking arousal from skin conductance using both binary- and continuous-valued features. The results obtained on experimental data sets demonstrate its ability to estimate arousal during different types of stress and in studies examining the human fear response. Our method also has the advantage of not requiring external labels. Annotation labels are

often expensive to obtain and may not necessarily be available in certain types of skin conductance-based experiments.

Future work would include incorporating EKG as yet another point process into the model. Moreover, the method used here relied on peak detection for locating SCRs. A sparse deconvolution scheme such as described in [15], [78]–[80] could be employed to recover the underlying sudomotor nerve activity and used for finding m_k instead of relying on simple peak detection. Furthermore, neuropsychiatric disorders such as PTSD and panic attacks give rise to heightened fear responses and it would be interesting to study data from these patients using the methods presented here. A complete experiment examining the human fear response typically includes the fear learning, fear recall and fear extinction phases. Only skin conductance signals from the fear learning stage were available in the data set used here. Examining how a fear state evolves over fear recall and fear extinction stages using the state-space method may help provide additional insight into certain types of neuropsychiatric disorders.

REFERENCES

[1] M. R. Roxo *et al.*, "The limbic system conception and its historical evolution," *Sci. World J.*, vol. 11, pp. 2427–2440, 2011.

[2] J. T. Cacioppo, L. G. Tassinary, and G. G. Berntson, *Handbook of Psychophysiology*. Cambridge, U.K.: Cambridge Univ. Press, 2007.

[3] F. Ringeval *et al.*, "Introducing the RECOLA multimodal corpus of remote collaborative and affective interactions," in *Proc. 10th IEEE Int. Conf. Workshops Autom. Face Gesture Recognit.*, 2013, pp. 1–8.

[4] J. A. Russell, "Evidence of convergent validity on the dimensions of affect," *J. Personality Social Psychol.*, vol. 36, no. 10, pp. 1152–1168, 1978.

[5] L. He *et al.*, "Multimodal affective dimension prediction using deep bidirectional long short-term memory recurrent neural networks," in *Proc. 5th Int. Workshop Audio/Visual Emotion Challenge*, 2015, pp. 73–80.

[6] M. Kächele *et al.*, "Ensemble methods for continuous affect recognition: Multi-modality, temporality, and challenges," in *Proc. 5th Int. Workshop Audio/Visual Emotion Challenge*, 2015, pp. 9–16.

[7] R. Weber *et al.*, "High-level geometry-based features of video modality for emotion prediction," in *Proc. 6th Int. Workshop Audio/Visual Emotion Challenge*, 2016, pp. 51–58.

[8] B. Sun *et al.*, "Exploring multimodal visual features for continuous affect recognition," in *Proc. 6th Int. Workshop Audio/Visual Emotion Challenge*, 2016, pp. 83–88.

[9] F. Povolny *et al.*, "Multimodal emotion recognition for AVEC 2016 challenge," in *Proc. 6th Int. Workshop Audio/Visual Emotion Challenge*, 2016, pp. 75–82.

[10] S. Koelstra *et al.*, "DEAP: A database for emotion analysis using physiological signals," *IEEE Trans. Affect. Comput.*, vol. 3, no. 1, pp. 18–31, Jan.–Mar. 2012.

[11] M. Soleymani *et al.*, "A multimodal database for affect recognition and implicit tagging," *IEEE Trans. Affect. Comput.*, vol. 3, no. 1, pp. 42–55, Jan.–Mar. 2012.

[12] D. McFarland, *A Dictionary of Animal Behaviour*. New York, NY, USA: Oxford Univ. Press, 2014.

[13] M. Benedek and C. Kaernbach, "Decomposition of skin conductance data by means of nonnegative deconvolution," *Psychophysiology*, vol. 47, no. 4, pp. 647–658, 2010.

[14] S. Jain *et al.*, "A compressed sensing based decomposition of electrodermal activity signals," *IEEE Trans. Biomed. Eng.*, vol. 64, no. 9, pp. 2142–2151, Sep. 2017.

[15] M. R. Amin and R. T. Faghih, "Sparse deconvolution of electrodermal activity via continuous-time system identification," *IEEE Trans. Biomed. Eng.*, vol. 66, no. 9, pp. 2585–2595, Sep. 2019.

[16] W. Boucsein, *Electrodermal Activity*. New York, NY, USA: Springer, 2012.

[17] J. J. Braithwaite *et al.*, "A guide for analysing electrodermal activity (EDA) & skin conductance responses (SCRs) for psychological experiments," *Psychophysiology*, vol. 49, no. 1, pp. 1017–1034, 2013.

[18] Y. Nagai *et al.*, "Activity in ventromedial prefrontal cortex covaries with sympathetic skin conductance level: A physiological account of a 'default mode' of brain function," *Neuroimage*, vol. 22, no. 1, pp. 243–251, 2004.

[19] M. M. Shanechi *et al.*, "A real-time brain-machine interface combining motor target and trajectory intent using an optimal feedback control design," *PloS One*, vol. 8, no. 4, 2013, Art. no. e59049.

[20] M. M. Shanechi *et al.*, "Feedback-controlled parallel point process filter for estimation of goal-directed movements from neural signals," *IEEE Trans. Neural Syst. Rehabil. Eng.*, vol. 21, no. 1, pp. 129–140, Jan. 2013.

[21] E. N. Brown *et al.*, "A statistical paradigm for neural spike train decoding applied to position prediction from ensemble firing patterns of rat hippocampal place cells," *J. Neurosci.*, vol. 18, no. 18, pp. 7411–7425, 1998.

[22] R. Barbieri *et al.*, "Dynamic analyses of information encoding in neural ensembles," *Neural Comput.*, vol. 16, no. 2, pp. 277–307, 2004.

[23] A. C. Smith *et al.*, "Dynamic analysis of learning in behavioral experiments," *J. Neurosci.*, vol. 24, no. 2, pp. 447–461, 2004.

[24] A. C. Smith *et al.*, "Analysis and design of behavioral experiments to characterize population learning," *J. Neurophysiol.*, vol. 93, no. 3, pp. 1776–1792, 2005.

[25] M. M. Shanechi *et al.*, "A brain-machine interface for control of medically-induced coma," *PLoS Comput. Biol.*, vol. 9, no. 10, 2013, Art. no. e1003284.

[26] R. Barbieri and E. N. Brown, "Analysis of heartbeat dynamics by point process adaptive filtering," *IEEE Trans. Biomed. Eng.*, vol. 53, no. 1, pp. 4–12, Jan. 2006.

[27] L. Citi, E. N. Brown, and R. Barbieri, "A real-time automated point-process method for the detection and correction of erroneous and ectopic heartbeats," *IEEE Trans. Biomed. Eng.*, vol. 59, no. 10, pp. 2828–2837, Oct. 2012.

[28] G. Valenza *et al.*, "Revealing real-time emotional responses: A personalized assessment based on heartbeat dynamics," *Sci. Rep.*, vol. 4, 2014, Art. no. 4998.

[29] M. J. Prerau *et al.*, "A mixed filter algorithm for cognitive state estimation from simultaneously recorded continuous and binary measures of performance," *Biol. Cybern.*, vol. 99, no. 1, pp. 1–14, 2008.

[30] M. J. Prerau *et al.*, "Characterizing learning by simultaneous analysis of continuous and binary measures of performance," *J. Neurophysiol.*, vol. 102, no. 5, pp. 3060–3072, 2009.

[31] T. P. Coleman *et al.*, "A mixed-filter algorithm for dynamically tracking learning from multiple behavioral and neurophysiological measures," in *The Dynamic Brain: An Exploration of Neuronal Variability and Its Functional Significance*. New York, NY, USA: Oxford Univ. Press, 2011, pp. 3–28.

[32] M. J. Prerau *et al.*, "Tracking the sleep onset process: An empirical model of behavioral and physiological dynamics," *PLoS Comput. Biol.*, vol. 10, no. 10, 2014, Art. no. e1003866.

[33] M. J. Prerau *et al.*, "Sleep neurophysiological dynamics through the lens of multitaper spectral analysis," *Physiology*, vol. 32, no. 1, pp. 60–92, 2016.

[34] K. F. K. Wong *et al.*, "Bayesian analysis of trinomial data in behavioral experiments and its application to human studies of general anesthesia," in *Proc. Annu. Int. Conf. IEEE Eng. Med. Biol. Soc.*, 2011, pp. 4705–4708.

[35] P. L. Purdon *et al.*, "Electroencephalogram signatures of loss and recovery of consciousness from propofol," *Proc. Nat. Acad. Sci. USA*, vol. 110, pp. E1142–E1151, 2013.

[36] D. S. Wickramasuriya, C. Qi, and R. T. Faghih, "A state-space approach for detecting stress from electrodermal activity," in *Proc. 40th Annu. Int. Conf. IEEE Eng. Med. Biol. Soc.*, 2018, pp. 3562–3567.

[37] J. Birjandtalab *et al.*, "A non-EEG biosignals dataset for assessment and visualization of neurological status," in *Proc. IEEE Int. Workshop Signal Process. Syst.*, 2016, pp. 110–114.

[38] A. L. Goldberger *et al.*, "PhysioBank, PhysioToolkit, and PhysioNet: Components of a new research resource for complex physiologic signals," *Circulation*, vol. 101, no. 23, pp. e215–e220, 2000.

[39] G. Fink, "Stress, definitions, mechanisms, and effects outlined: Lessons from anxiety," in *Stress: Concepts, Cognition, Emotion, and Behavior*, 1st ed. San Diego, CA, USA: Academic, 2016, pp. 3–11.

[40] H. D. Critchley, "Electrodermal responses: What happens in the brain," *Neuroscientist*, vol. 8, no. 2, pp. 132–142, 2002.

[41] S. D. Kreibig, "Autonomic nervous system activity in emotion: A review," *Biol. Psychol.*, vol. 84, no. 3, pp. 394–421, 2010.

[42] Y. Dai *et al.*, "Reputation-driven multimodal emotion recognition in wearable biosensor network," in *Proc. IEEE Int. Instrum. Meas. Technol. Conf.*, 2015, pp. 1747–1752.

[43] D. R. Bach *et al.*, "PsPM-HRA1: Skin conductance responses in fear conditioning with visual CS and electrical US," Feb. 2017. [Online]. Available: https://doi.org/10.5281/zenodo.321641
[44] D. R. Bach *et al.*, "Dynamic causal modelling of anticipatory skin conductance responses," *Biol. Psychol.*, vol. 85, no. 1, pp. 163–170, 2010.
[45] M. Staib *et al.*, "Optimising a model-based approach to inferring fear learning from skin conductance responses," *J. Neurosci. Methods*, vol. 255, pp. 131–138, 2015.
[46] M. B. L. Careaga *et al.*, "Understanding posttraumatic stress disorder through fear conditioning, extinction and reconsolidation," *Neurosci. Biobehav. Rev.*, vol. 71, pp. 48–57, 2016.
[47] W. T. Roth *et al.*, "Skin conductance habituation in panic disorder patients," *Biol. Psychiatry*, vol. 27, no. 11, pp. 1231–1243, 1990.
[48] M. R. Milad *et al.*, *Fear Conditioning in Rodents and Humans*. Totowa, NJ, USA: Humana Press, 2011, pp. 111–132.
[49] J. J. Quinn and M. S. Fanselow, "Defenses and memories: Functional neural circuitry of fear and conditional responding," in *Fear and Learning: From Basic Processes to Clinical Implications*. Washington, DC, USA: Amer. Psychol. Assoc., 2006, pp. 55–74.
[50] M. Asahina *et al.*, "Sweating on the palm and sole: Physiological and clinical relevance," *Clin. Auton. Res.*, vol. 25, no. 3, pp. 153–159, 2015.
[51] O. V. Lipp, "Human fear learning: Contemporary procedures and measurement," in *Fear and Learning: From Basic Processes to Clinical Implications*. Washington, DC, USA: Amer. Psychol. Assoc., 2006, pp. 37–51.
[52] S. Doberenz *et al.*, "Methodological considerations in ambulatory skin conductance monitoring," *Int. J. Psychophysiol.*, vol. 80, no. 2, pp. 87–95, 2011.
[53] A. Greco *et al.*, "cvxEDA: A convex optimization approach to electrodermal activity processing," *IEEE Trans. Biomed. Eng.*, vol. 63, no. 4, pp. 797–804, Apr. 2016.
[54] A. C. Smith and E. N. Brown, "Estimating a state-space model from point process observations," *Neural Comput.*, vol. 15, no. 5, pp. 965–991, 2003.
[55] P. McCullagh and J. A. Nelder, *Generalized Linear Models*, vol. 37. Boca Raton, FL, USA: CRC Press, 1989.
[56] D. E. Aikins *et al.*, "Thought suppression failures in combat PTSD: A cognitive load hypothesis," *Behav. Res. Therapy*, vol. 47, no. 9, pp. 744–751, 2009.
[57] L. L. Munro *et al.*, "Electrodermal lability and rapid vigilance decrement in a degraded stimulus continuous performance task," *J. Psychophysiol.*, vol. 1, pp. 249–257, 1987.
[58] J. C. Laberg and B. Ellertsen, "Psychophysiological indicators of craving in alcoholics: Effects of cue exposure," *Brit. J. Addiction*, vol. 82, no. 12, pp. 1341–1348, 1987.
[59] K. Kallinen and N. Ravaja, "Emotion-related effects of speech rate and rising vs. falling background music melody during audio news: The moderating influence of personality," *Personality Individual Differences*, vol. 37, no. 2, pp. 275–288, 2004.
[60] L. M. Gatzke-Kopp *et al.*, "Serious delinquent behavior, sensation seeking, and electrodermal arousal," *J. Abnormal Child Psychol.*, vol. 30, no. 5, pp. 477–486, 2002.
[61] J. G. Beck *et al.*, "Rebound effects following deliberate thought suppression: Does PTSD make a difference?" *Behav. Therapy*, vol. 37, no. 2, pp. 170–180, 2006.
[62] B. D. Smith, "Extraversion and electrodermal activity: Arousability and the inverted-U," *Personality Individual Differences*, vol. 4, no. 4, pp. 411–419, 1983.
[63] D. R. Bach *et al.*, "Modelling event-related skin conductance responses," *Int. J. Psychophysiol.*, vol. 75, no. 3, pp. 349–356, 2010.
[64] N. Mella *et al.*, "The role of physiological arousal in time perception: Psychophysiological evidence from an emotion regulation paradigm," *Brain Cogn.*, vol. 75, no. 2, pp. 182–187, 2011.
[65] C. Lithari *et al.*, "Are females more responsive to emotional stimuli? A neurophysiological study across arousal and valence dimensions," *Brain Topography*, vol. 23, no. 1, pp. 27–40, 2010.
[66] J. M. Mendel, *Lessons in Estimation Theory for Signal Processing, Communications, and Control*. London, U.K.: Pearson Educ., 1995.
[67] P. D. Jong and M. J. Mackinnon, "Covariances for smoothed estimates in state space models," *Biometrika*, vol. 75, no. 3, pp. 601–602, 1988.
[68] A. O. Hamm and A. I. Weike, "The neuropsychology of fear learning and fear regulation," *Int. J. Psychophysiol.*, vol. 57, no. 1, pp. 5–14, 2005.
[69] M. Fredrikson and A. Öhman, "Cardiovascular and electrodermal responses conditioned to fear-relevant stimuli," *Psychophysiology*, vol. 16, no. 1, pp. 1–7, 1979.
[70] U. T. Eden *et al.*, "Dynamic analysis of neural encoding by point process adaptive filtering," *Neural Comput.*, vol. 16, no. 5, pp. 971–998, 2004.
[71] S. Moratti *et al.*, "Hypofunction of right temporoparietal cortex during emotional arousal in depression," *Arch. Gen. Psychiatry*, vol. 65, no. 5, pp. 532–541, 2008.
[72] A. L. Mahan and K. J. Ressler, "Fear conditioning, synaptic plasticity and the amygdala: Implications for posttraumatic stress disorder," *Trends Neurosci.*, vol. 35, no. 1, pp. 24–35, 2012.
[73] D. S. Wickramasuriya, M. R. Amin, and R. T. Faghih, "Skin conductance as a viable alternative for closing the deep brain stimulation loop in neuropsychiatric disorders," *Front. Neurosci.*, vol. 13, 2019, Art. no. 780.
[74] A. Sano *et al.*, "Multimodal ambulatory sleep detection using LSTM recurrent neural networks," *IEEE J. Biomed. Health Inform.*, vol. 23, no. 4, pp. 1607–1617, Jul. 2019.
[75] M. Zaheer *et al.*, "Latent LSTM allocation joint clustering and non-linear dynamic modeling of sequential data," in *Proc. 34th Int. Conf. Mach. Learn.*, 2017, vol. 70, pp. 3967–3976.
[76] X. Zheng *et al.*, "State space LSTM models with particle MCMC inference," 2017, *arXiv:1711.11179*.
[77] R. G. Krishnan *et al.*, "Structured inference networks for nonlinear state space models," in *Proc. 31st AAAI Conf. Artif. Intell.*, 2017, pp. 2101–2109.
[78] M. R. Amin and R. T. Faghih, "Inferring autonomic nervous system stimulation from hand and foot skin conductance measurements," in *Proc. 52nd Asilomar Conf. Signals, Syst. Comput.*, Oct. 2018, pp. 655–660.
[79] R. T. Faghih *et al.*, "Characterization of fear conditioning and fear extinction by analysis of electrodermal activity," in *Proc. 37th Annu. Int. Conf. IEEE Eng. Med. Biol. Soc.*, 2015, pp. 7814–7818.
[80] R. T. Faghih, "From physiological signals to pulsatile dynamics: A sparse system identification approach," in *Dynamic Neuroscience*. New York, NY, USA: Springer, 2018, pp. 239–265.